DOI:
10.1016/j.jnutbio.2020.108364

Document Version
Peer reviewed version

Creb-Pgc1α pathway modulates the interaction between lipid droplets and mitochondria and influences high fat diet-induced changes of lipid metabolism in the liver and isolated hepatocytes of yellow catfish

Yu–Feng Song [a], Christer Hogstrand [c], Shi-Cheng Ling [a], Guang-Hui Chen [a], Zhi Luo [a, b,*]

[a] *Key Laboratory of Freshwater Animal Breeding, Ministry of Agriculture, Fishery College, Huazhong Agricultural University, Wuhan 430070, China*

[b] *Laboratory for Marine Fisheries Science and Food Production Processes, Qingdao National Laboratory for Marine Science and Technology, Qingdao 266237, China*

[c] *Diabetes and Nutritional Sciences Division, School of Medicine, King's College London, Franklin-Wilkins Building, 150 Stamford Street, London, SE1 9NH, UK*

Corresponding author. Prof. Zhi Luo, Tel.: +86-27-8728-2113; Fax: +86-27-8728-2114; Email address: luozhi99@mail.hzau.edu.cn; luozhi99@aliyun.com (Z. Luo).

Abstract

Although the crucial role of lipid droplets (LDs), mitochondria (MT) and their interactions in regulating lipid metabolism are well accepted, the mechanism of LDs-MT interactions in high fat diet (HFD)-induced changes of lipid metabolism remains unknown. Thus, this study was conducted to determine the mechanism of LDs-MT interactions in HFD-induced changes of lipid accumulation. We found that HFD not only up-regulated the expression of key proteins linked with TAG biosynthesis, but also increased the expression of proteins involved in lipolysis and fatty acid (FA) oxidation in LDs, including Rab32 (the only Rab protein associated with the MT). FA-induced LDs accumulation coincided with increased mitochondrial biogenesis, suggesting the potential LDs-MT interaction in hepatocytes after FA incubation. Also, FA incubation markedly increased the localization of Rab32 into LDs and MT, which confirmed the LDs-MT interaction and indicated the involvement of Rab32 in LDs-MT interaction following FA incubation. Inhibitors of Creb-Pgc1α pathway significantly blocked the localization of Rab32 into LDs and MT, and significantly reduced FA-induced LDs lipolysis by targeting Atgl and Plin5. Meanwhile, the FA-enhanced LDs accumulation, and mitochondrial biogenesis, fusion and oxidation were also significantly repressed. These indicated the regulatory role of Creb-Pgc1α in Rab32-mediated LDs-MT interactions and lipolysis after FA incubation. Taken together, these results revealed a novel mechanism of HFD- and FA-induced LDs-MT interactions in regulating hepatic LDs lipolysis, which provided new insight into the crosstalk between LDs-MT interaction and their potential role in HFD-induced hepatic steatosis.

Graphical abstract

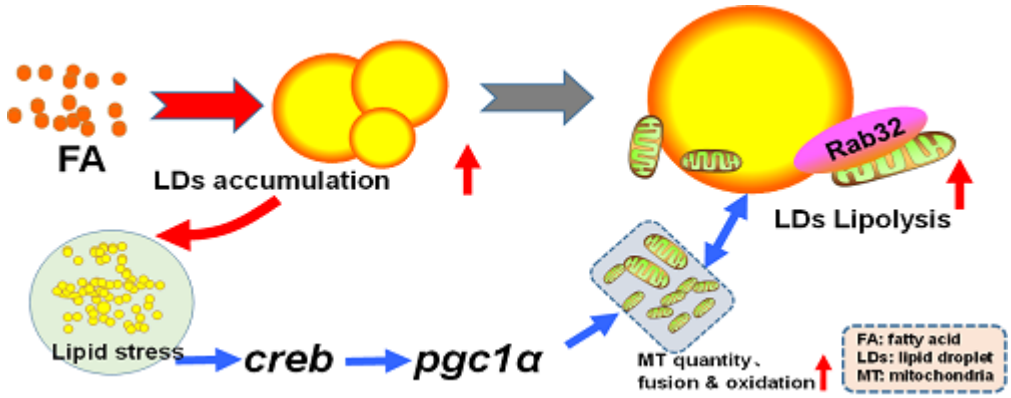

Keywords: Creb-Pgc1α pathway; Rab32; LDs-MT interaction; Lipid metabolism; High fat diet

Abbreviations: Acadm, acyl-CoA dehydrogenase; Acox1, acyl-CoA oxidase 1; Atgl, adipose tissue glycerol lipase; Adrp, Perilipin-2; APO-1, Apolipoprotein-1; CD36, CD36 antigen; COX, cyclooxygenase; Cpt, carnitine O-palmitoyltransferase; Creb, Cyclic amp (cAMP) response element binding protein; DAG, diacylglycerol; Dgat1, diacylglycerol O-acyltransferase; FA, fatty acid; Fabp, fatty acid-binding protein; Fis1, mitochondrial fission 1 protein; GI, glycerine; HFD, high fat diet; LDs, lipid droplets; LDL-R, low density lipoprotein receptor; LDPs, lipid droplet proteins; Mfn1, mitofusin 1; Mid, mitochondrial dynamics proteins; MMP, mitochondrial membrane potential; MT, mitochondria; Nrf1, nuclear respiratory factor 1; OA, oleic acid; PA, palmitic acid; Pgc-1α, peroxisome proliferator-activated receptor γ (PPARγ) coactivator-1α; Plin5, perilipin-5; Rab, Ras-related protein; TAG, triacylglycerol; Tfam, transcription factor A; Tfb1m, mitochondrial

transcription factor B1; VLDL-R, very low density lipoprotein receptor.

1. Introduction

Nowadays high fat diet (HFD)-induced hepatic steatosis, as the most common chronic liver disease for human being[1], increases rapidly worldwide [2]. Steatosis is characterized by excessive lipid droplets (LDs) accumulation in hepatocytes. LDs consist of a neutral lipid core covered with a phospholipid monolayer membrane and proteins [3]. It was initially considered an inert particle for intracellular lipid storage. However, recently increasing evidences show that LDs are metabolically active organelles and play a pivotal role in cellular lipid metabolism [4]. Meantime, LDs possesses complex interaction with other organelles, especially with mitochondria (MT) [4]. LDs and MT are two essential organelles for the regulation of lipid homeostasis, and their dysfunction is related to hepatic steatosis [5, 6]. However, although the close physical and functional interactions between LDs and MT are well accepted [7], it is not yet clear about the mechanism of LDs-MT interactions on HFD-mediated changes of lipid metabolism.

Mitochondrial programs are complex processes requiring the coordinated expression and assembly of ~1,500 proteins [8]. Among these proteins, the transcriptional coactivator Pgc1α is a master regulator of mitochondrial biogenesis [9]. It also acts as a global regulator of metabolism and regulates the expression of LD-related proteins in hepatocytes [10, 11]. Thus, it is reasonable to speculate the potential regulatory role of Pgc1α in LDs-MT interactions. On the other hand, the coactivator of Creb (TORC) is the most potent activator

for Pgc1α [12]. Creb regulates lipid metabolism and mediates mitochondrial gene expression [13, 14], implying the bridging function of Creb for linking lipid metabolism and MT function.

Rab proteins are generally known as GTPase switches and control membrane trafficking among intracellular compartments [15]. They are also associated with intracellular lipid accumulation [16]. Members of the Rab family have been consistently identified in proteomic screens of LDs [17]. Several studies reported that Rabs regulated the interaction between LDs and MT [18], and that Rabs were the mediators involved in the LDs-MT interaction [19]. In addition, Rab32 is the only Rab GTPase associated with the MT [20]. However, whether Rab32 regulated HFD-mediated LDs-MT interactions remained to be investigated.

Fish are the by far the largest group of vertebrates in the world. During the evolution of vertebrates, the entire genome was duplicated twice. However, fish have a third genome duplication, called the fish-specific genome duplication (FSGD) [21]. The FSGD has been observed in yellow catfish (*Pelteobagrus fulvidraco*), freshwater teleost widely distributed in China and other countries[22]. Some duplicated genes evolved new functions that in turn resulted in novel regulatory mechanisms [21]. Moreover, yellow catfish frequently exhibits excessive hepatic lipid accumulation after HFD feeding, which have an adverse effect on growth performance and health [23]. Therefore, using yellow catfish as a model, we hoped to find some novel regulatory mechanism of lipid metabolism. Our previous studies found that excessive LDs accumulation coincided with the increase in abundance of swelling and vesiculation of MTs in the liver [24, 25], suggesting the potential role of LDs-MT

interactions, but the underlying mechanisms remained unknown. Thus, the purpose of this study was to test the mechanism of LDs-MT interactions in HFD-induced changes of hepatic lipid metabolism in *P. fulvidraco*. Our present study reveals an important regulatory role of Creb-Pgc1α pathway in HFD-mediated LDs-MT interactions, and suggests that the Creb-Pgc1α pathway controls HFD-induced changes of lipid metabolism via targeting two key proteins: Atgl, the rate-limiting enzyme in triacylglycerol (TAG) hydrolysis [26], and Plin5, a LD targeting protein who regulates lipolysis and FA oxidation [27].

2. Materials and methods

2.1. Experimental treatments

The present study consisted of four experiments. Exp. 1 was conducted to analyze the sub-proteome profiles of hepatocellular LDs from *P. fulvidraco* fed the control or HFD. Exp. 2 was conducted to explore the effect of FA incubation on LDs-MT interaction in primary hepatocytes from *P. fulvidraco*. Exp. 3 was conducted to explore the mechanism of LDs-MT interaction in FA-induced alteration of lipid metabolism. Exp. 4 was conducted to investigate the effect and mechanism of FA incubation on mitochondrial biogenesis and lipid metabolism of human liver cancer cell lines (HepG2), and explore the potentiality of extrapolating the results in yellow catfish to human.

The present experimental protocols in animals and cells were approved by the Ethics Committee of Huazhong Agricultural University.

2.1.1. Exp. 1: in vivo, analyzing sub-proteome profiles of hepatocellular LDs from P.

fulvidraco fed the control and HFD

Ingredients and feed formulation for two experiments diets were shown in our parallel studies ([28], Supplementary Table 1). Dietary fat levels was 11.3% for the control and 15.4% for the HFD group, respectively. According to our pilot study, 15.4% of dietary lipid adversely influenced growth performance and resulted in steatosis of *P. fulvidraco*, and was considered to be HFD. Each diet was fed to three replicate tanks of yellow catfish (initial mean body weight: 3.8 ± 0.2 g), with 30 fish per tank. The feeding experiment continued for 8 wk. The details feeding and culture management were shown in our parallel study [28].

Before sampling, fish were starved for 24 h to avoid prandial effects, and then euthanized with MS-222 (tricaine methanesulfonate, 100 mg/l). Fish were randomly collected, weighed and dissected on ice to obtain the liver samples. In order to analyze hepatocellular LDs sub-proteome, liver samples were removed, based on the protocols described in Liu et al [17]. For analysis of Oil Red O staining, western blotting and mRNA expression, samples were removed immediately, frozen in liquid nitrogen and then stored at -80 °C for further analysis.

2.1.2. Exp. 2: investigating the FA-induced alteration of LDs and MT in primary hepatocytes of P. fulvidraco

Primary hepatocytes were isolated from *P. fulvidraco* and cultured as previously described [24, 25]. In order to explore the effect of FA on LDs-MT interaction, we investigated the quantitative change of LDs and MT in hepatocytes from *P. fulvidraco* after FA incubation. FA consisted of oleic acid (OA) and palmitic acid (PA) at a ratio of 1:1. They

were dissolved in DMSO before addition. The total concentration of OA and PA was 1 mM. The concentrations FA was selected according to previous report [28] and our pilot trial. Two groups were designed: control (containing 0.1% DMSO) and FA medium (1 mM). Each treatment was performed in quadruplicate. The cells were gathered for the following analysis after 0h, 24h and 48 h, respectively.

2.1.3. Exp. 3: exploring the mechanism of LDs-MT interaction in regulating FA-induced changes of LDs lipolysis

Primary hepatocytes were isolated and cultured as described in Exp. 2. The specific inhibitors for Creb-Pgc1α pathway (666-15 for Creb and SR-18292 for Pgc1α) and activator (ZLN005) for Creb-Pgc1α pathway were used to test the role of Creb-Pgc1α pathway on FA-induced change of mitochondrial biogenesis and lipolytic metabolism. For the Creb inhibition experiment, four groups were designed: control (containing 0.1% DMSO), 666-15 (15 μM), FA (1 mM), 666-15 (15 μM) + FA (1 mM), respectively. The experimental protocols for SR-18292 inhibitor and ZLN005 activator experiments were similar to those in the 666-15 treatment above. Each treatment was performed in quadruplicate. The concentrations of 666-15 (15 μM), SR-18292 (20 μM) and ZLN005 (5 μM) were selected according to previous experiments [29-31] and our pilot trial. The specific inhibitors/or activator were added 2 h prior to the addition of FA. The cells were gathered for the following analysis after 0h, 24h and 48 h, respectively.

2.1.4. Exp. 4: explore the mechanism of FA incubation influencing mitochondrial biogenesis and lipid metabolism of human liver cancer cell line (HepG2)

The HepG2 cell lines were cultured as described in our previous study [30]. Two groups were designed: control (containing 0.1% DMSO) and FA medium (0.5 mM). FA consisted of oleic acid (OA) and palmitic acid (PA) at a ratio of 1:1. The total concentration of OA and PA was 0.5 mM. The concentrations of FA were selected according to previous experiments [32] and our pilot trial. Each treatment was performed in quadruplicate. The cells were gathered for the following analysis after 0h, 24h and 48 h, respectively.

2.2. Sample analysis

2.2.1. Histochemical and ultrastructural analyses

Histochemical and ultrastructural observations for livers and hepatocytes were conducted according to the methods described in our previous studies [24, 25]. The quantified area of LDs in the Oil Red O observation were evaluated by Image J software [24, 25].

2.2.2. Confocal imaging

Confocal imaging were conducted according to the methods described in our previous studies [24, 25]. Primary hepatocytes were plated on coverslips in 12-well plates and transfected with the indicated plasmids. After FA treatment, coverslips were washed once with PBS and fixed in 4% formaldehyde for 10 min. Cells were permeabilized for 15 min at room temperature in a staining buffer containing Triton X-100 (0.1%) in PBS and then incubated with DAPI for 10 min. The coverslips were then washed with PBS twice and fixed on slides. Images were captured by ANDOR laser scanning confocal microscope (ANDOR Microscopy Systems).

187 *2.2.3. Isolation of LDs, LC-MS/MS and data analysis*

188 LDs isolation was performed as described in Liu et al [17]. 4 g of liver was pooled
189 from three fish each tank. Tissues were cut into tiny pieces and washed twice in PBS. The
190 pellet was disrupted in 2.5 ml lysis buffer A [50 mM Tris-HCl (pH 7.4), 1 mM DTT, 250
191 mM sucrose, 5 mM $MgCl_2$, 25 g/ml spermidine, 1 mM PMSF] using a SPAN bomb (Parr
192 Instrument Company, Moline, 1 L) for 15 min under 500 psi nitrogen. The lysate was
193 centrifuged for 10 min at 1,000g at 4°C. The supernatant was mixed with buffer B (20 mM
194 HEPES, 10 mM KCl, 2 mM $MgCl_2$) (at a ratio of 1:1) and centrifuged for 4 h at 154,000 g in
195 a Beckman SW41Ti rotor at 4 °C. Buoyant fraction (LDs) was washed twice with buffer B
196 and then resuspended in a 2 × volume of buffer B.

197 Protein samples and trypsin digestion were performed as described in Liu et al [17].
198 Briefly, whole tissue proteins and cells were extracted with urea lysis buffer and measured
199 with Bradford assay according to manufacturer's instructions. Protein samples were digested
200 with trypsin at a mass ratio of 1:50 enzyme/protein overnight at 37 °C and the reaction was
201 stopped by the addition of 3 μl of formic acid to a final concentration 1%. LD protein was
202 extracted from the LD fraction with SDS-PAGE loading buffer. As for SDS-PAGE
203 separation, 20 μg LD protein and whole tissue proteins were prepared for by in-gel digestion,
204 based on published protocols [33].

205 iTRAQ labeling, LC-MS/MS and data analysis were performed according to our
206 methods described previously [34]. Briefly, protein concentrations were established using a
207 Bradford assay, with protein samples digested with trypsin solution overnight at 37 °C and
208 labeled with iTRAQ reagents (8-plex; AB SCIEX, Massachusetts, USA) according to the

manufacturer's instructions. Then, typical peptides labeled with 8-plex iTRAQ tags were pooled and dried. The peptides were separated on a Shimadzu LC-20AB HPLC Pump system coupled with a high pH RP column. The peptides were reconstituted with buffer A (5% ACN, 95% H_2O, pH 9.8) to 2 ml and loaded into a column containing 5-μm particles (Phenomenex). The peptides were separated at a flow rate of 1 mL/min with a gradient of 5% buffer B (5% H_2O, 95% ACN, pH 9.8) for 10 min, 5–35% buffer B for 40 min, 35–95% buffer B for 1 min. The system was then maintained in 95% buffer B for 3 min and reduced to 5% within 1 min before equilibrating with 5% buffer B for 10 min. Elution was monitored by measuring absorbance at 214 nm, and fractions were collected every minute. The eluted peptides were pooled as 20 fractions and vacuum-dried. Next, the mass spectrometry analysis was performed as described in Michalski et al [35], using Q-Exactive mass spectrometer (Thermo Fisher Scientific, San Jose, CA), coupling with LC-20AD (Shimadzu). The software IQuant was used to quantify the labeled peptides with isobaric tags. To assess the confidence of peptides, the PSMs were pre-filtered at a PSM-level false discovery rate (FDR) of 1%. Based on the “simple principle” (the parsimony principle), identified sequences of peptide were assembled into a set of confident proteins.

Three biological replicates were set for better coverage of the target proteome with reliable statistical consistency. A 95% confidence interval (CI) was set as the significant threshold for protein identification. Quality control (QC) was performed to determine if a re-analysis step was needed. All the proteins with a FDR < 1% proceeded with downstream analysis, including Gene Ontology (GO), COG and Pathway. Furthermore, we also performed the in-depth analysis based on differentially expressed proteins, including GO

enrichment analysis, KEGG pathway enrichment analysis and cluster analysis. The protein lists from the 20 LC-MS/MS runs, obtained by fractionation of the iTRAQ pooled sample, were merged. The confidence level of each differentially expressed protein was calculated as a P-value using ProteinPilot, allowing the results to be evaluated, not only based on the magnitude of the change but also on the confidence level of the change. GO was performed using the bioinformatics analysis tool DAVID (http://david. abcc.ncifcrf.gov) to determine the functional classifications of the iTRAQ-identified proteins.

2.2.4. Western blotting

Western blotting was performed according to our previous study [28]. 25μg protein was separated on 12.5% SDS-polyacrylamide gels. After SDS-PAGE, the proteins were transferred to a PVDF membrane, and then blocked with 8% (w/v) milk for 1 h. The membrane was incubated with antibodies against Adrp (15294-1-AP; ProteinTech, Chicago, Illinois, USA), Gm130 (ab30637; Abcam, Cambridge, MA, USA), Calnexin (ab10286), Cox IV (ab33985), Gapdh (ab9485), Atgl (ab99532), Plin5 (ab222811), Creb (ab31387), Pgc1α (ab84139), Rab32 (ab229604), Cd36 (ab64014), Dgat1 (ab54037), Cox-1 (ab109025) and Mfn-1 (ab221661) overnight at 4 °C, and then processed with goat anti-rabbit IRDye 800CW secondary antibody, (926-32211; Li-Cor Biosciences, Lincoln, NE, USA). The protein bands were visualized with an Odyssey Infrared Fluorescent Western Blots Imaging System (Li-Cor Bioscience) and quantified by Image-Pro Plus 6.0.

2.2.5. Confocal immunofluorescence analysis

Confocal immunofluorescence analysis was performed according to previous study [36].

Briefly, cells were washed with PBS, and fixed with 1% paraformaldehyde for 1 h at room temperature. They were then washed with PBS, and permeabilised in 0.1% saponin, 20 mM glycine in PBS (SPBSG) for 30 min. Subsequently, polyclonal anti-Rab32 antiboby (1:10 dilution) and monoclonal marker anti-bodies in 0.1% saponin/PBS (SPBS) were incubated with primary antibody. Cells were washed in SPBS, and specific labelling was detected by subsequent incubation with 50 µl of FITC-or Texas Red-conjugated Affinipure goat anti-rabbit or goat anti-mouse IgG (10 mg/ml; Jackson ImmunoResearch Laboratories, Inc., West Grove, PA, USA) in SPBS for 1 h. After methanol dehydration, the cells were mounted in Mowiol (Sigma-Aldrich, the Netherlands) and examined using a confocal laser scanning microscope.

2.2.6. Flow cytometric analysis

Flow cytometric analysis was performed according to our previous study [28]. In brief, a FACSort (Becton Dickinson, Sunnyvale, CA) equipped with a single Argon ion laser was used according to the methods described previously [37]. Excitation was done at 488 nm and the emission filters used were 515-545 BP (green; FITC) and 600 LP (red; PI). A minimum of 5,000 cells per sample were analysed and data were stored in list mode. Electronic compensation was used to eliminate bleed through of fluorescence. Data analysis was performed with the standard Lysis and Cellfit software (Becton Dickinson).

2.2.7. Mitochondrial membrane potential (MMP) measurement

The fluorescent probe, JC-1 (Beyotime Biotech, Nanjing, China), was used to measure the MMP according to the manufacturer’s instructions, as described in our recent study [38].

The cells were incubated with JC-1 staining solution (5 μg/mL) for 20 min at 28 °C. Then cells were rinsed twice with JC-1 staining buffer and resuspended in 300 μl JC-1 staining buffer. Two laser lines (488 nm and 552 nm) were used to collect fluorescence images (green and red fluorescence) by fluorescence laser scanning confocal microscopy (Leica, Wetzlar, German). The MMP was calculated as the fluorescence ratio of green to red.

2.2.8. Contents of ATP, cAMP, lipid, TAG, diacylglycerol (DAG) and glycerine, and COX activity

ATP was measured using an ATP Assay Kit (Beyotime, Haimen, China) as describe in our previous study [38]. Assay of cAMP levels was performed according to our previous study [25] using the direct cAMP ELISA kit (Enzo Life Sciences). The contents of TAG, DAG and glycerine were determined according to our previous studies [24, 25] using TAG, DAG and glycerine Assay Kit (Jiancheng Biotech, Nanjing, China). Hepatic lipid content was determined by ether extraction according to our previous study [39]. COX activity was assayed using COX assay kit (Genmed, Shanghai, China) by measuring reduced cytochrome C consuming at 550 nm according to the methods described previously [38].

2.2.9. DNA isolation and real-time PCR (RT-PCR) for mtDNA

The mtDNA was isolated according to the methods described in Xin et al [40] using a commercial kit (MT DNA Isolation Kit, Biovision). mtDNA levels were measured with SYBR (Thermo Fisher Scientific, Waltham, MA, USA) green dye-based RT-PCR assay using ABI PRISM 7300 sequence detection system (Applied Biosystems, CA, USA) [41]. Primer sequence was yellow catfish NADH dehydrogenase 1 gene (mtDNA): forward

294 5’-GGAGCAGTAGCCCAAACAAT-3’ and reverse
295 5’-AGTGATAAGGGTGCAGAGGTT-3’. Plasmid DNA with complementary DNA
296 sequence for human mtDNA was obtained from OriGene Technologies (SC101172;
297 Rockville, MD, USA). Concentrations of plasma mtDNA were converted to copy number
298 via DNA copy number calculator [42]. Plasmid DNA was diluted in 10-fold serial dilutions
299 and measured as standard curve. All samples were measured with standards at the same time.

300 *2.2.10. mRNA level determination by real-time quantitative PCR (Q-PCR)*

301 Analyses on gene transcript levels were conducted by Q-PCR method described before
302 [24, 25]. The primer sequences used in this analysis are given in Supplementary Table 2. A
303 set of eight housekeeping genes (*β-actin*, *gapdh*, *ef1a*, *18s rna*, *hprt*, *b2m*, *tuba* and *rpl17*)
304 were selected from our transcriptome database to test their transcription stability. Our pilot
305 experiment indicated that *β-actin* and *gapdh* (M=0.28) showed the most stable level of
306 expression across the experimental conditions as suggested by geNorm [43]. Thus, the
307 relative expression levels were normalized to the geometric mean of the combination of
308 *β-actin* and *gapdh*, and calculated using the $2^{-\Delta\Delta Ct}$ method.

309 ***2.3. Statistical analysis***

310 All data were expressed as mean ± standard error of means (SEM). The normality of
311 data distribution and the homogeneity of variances were analyzed by the
312 Kolmogorov–Smirnov test and Bartlett’s test, respectively. Then, data were subjected to
313 one-way ANOVA and Tukey’s multiple range test. Differences between FA and FA+
314 inhibitor/activator groups (or between the control and HFD group) were analyzed by

Student's T-test for independent samples. All analysis were conducted with SPSS 19.0 software, and the minimum significance level was set at $P< 0.05$.

3. Results

3.1. Overview of differentially expressed LD proteins in the hepatocytes of yellow catfish fed the control and HFD

Compared to the control, HFD increased hepatic lipid accumulation, as shown in oil-red O staining and lipid content analysis; HFD also increased MT accumulation and up-regulated the mRNA abundances of LDL-R and VLDL-R (Supplementary Fig. 1).

To get an overview of differentially expressed LD proteins in the hepatocytes of *P. fulvidraco* fed the control and HFD, we analyzed the sub-proteome profile of LDs. First, in order to evaluate the purity of isolated LDs, we quantified the protein expression of several markers that were specific for intracellular organelles, such as Golgi complex (Gm130), endoplasmic reticulum (Calnexin), MT (Cox IV), and cytosols (Gapdh) in the isolated LDs by Western blotting (Supplementary Fig. 2). The expression of LDs marker, Adrp, was predominant in isolated LDs, but the protein expression of markers from other organelles was almost undetectable, indicating that our LDs possessed high purity and could be used for sub-proteome analysis. Then, we used iTRAQ to perform the sub-proteome analysis of LD proteins, and the results were shown in Supplementary Fig. 3. Overall, 856 proteins were enriched at 1% FDR and 87 of them were enriched greater than 5-fold in LDs. MS raw files have been submitted to ProteomeXchange (accession number: PXD013670). Consistent with

known functions, LD proteins were highly specialized in lipid metabolic processes. Compared to the control, HFD markedly up-regulated the expression of LD proteins who functioned in TAG biosynthesis, lipolysis and FA oxidation (Supplementary Fig. 4A & B), indicating that HFD not only accelerated TAG biosynthesis, but also enhanced lipolysis and FA oxidation. Among these differentially expressed LDs proteins, HFD up-regulated Atgl protein expression by more than 5-fold but down-regulated Plin5 protein expression by more than 5-fold, two key LDs proteins for lipolysis. Rab proteins are generally known as GTPase switches controlling membrane trafficking among intracellular compartments [44]. In the present study, HFD significantly up-regulated the expression of multiple Rab proteins in LDs, including Rab1, Rab5, Rab7, Rab10, Rab18 and Rab32. Among these Rab proteins from LD proteins, Rab32 was the only Rab GTPase associated with the MT [20], whose protein expression was significantly up-regulated by HFD.

We further verified the HFD-induced alteration of LDs proteins by Q-PCR and Western blotting. Compare to the control, HFD significantly up-regulated the protein levels of Rab32, Dgat1, Cd36 and Atgl, and also the mRNA abundance of key genes involved in lipid metabolism, including *fabp1*, *cd36*, *apo-a1*, *dgat1*, *agpat2*, *lclat1*, *atgl*, *cpt1* and *cpt2* (Fig. 1A, B & C). HFD up-regulated the mRNA abundance of *rab32* (the only Rab GTPase associated with the MT) but down-regulated the mRNA abundance of *plin5*. All these data showed a high consistency with LDs sub-proteome results. Taken together, our study indicated that HFD not only up-regulated TAG biosynthesis process, but also activated lipolysis and FA oxidation in LDs.

3.2. FA-induced hepatocellular LDs accumulation coincided with increased mitochondrial

biogenesis

We investigated the FA-induced change of LDs and MT in hepatocytes of *P. fulvidraco*. First, compared to the control, FA incubation significantly enhanced the volumes and diameter of LDs, in parallel with remarkable enhancement of mitochondrial fluorescence intensity (red) in hepatocytes (Fig. 2A-F). Second, EM observation found that FA incubation induced LDs accumulation and increased mitochondrial quantity (Fig. 2G-I). Meanwhile, FA incubation also increased the co-localization between MTs and LDs (Fig. 2J). Q-PCR analysis indicated that FA incubation markedly up-regulated the mRNA abundance of genes involved in mitochondrial biogenesis, including *creb*, *pgc-1α*, *tfam*, *nrf-1*, *nrf-2*, *tfb1m* and *tfb2m* (Fig. 2K). These data indicated that FA-induced hepatocellular LDs accumulation paralleled with the increase of mitochondrial biogenesis, suggesting the potential LDs-MT interaction under FA incubation.

3.3. FA up-regulated the expression of Creb and Pgc1α, and enhanced the localization of Rab32 into LDs and MT

FA markedly up-regulated the protein levels of Creb and Pgc1α, and the cAMP levels in hepatocytes (Fig. 3A-D), suggesting that FA activated the Creb- and Pgc1α-mediated pathways.

To further determine the role of Rab32 in FA-induced LDs-MT interactions, we tested the FA-induced changes of the Rab32 localization in LDs and MT. The co-localization analysis indicated that FA incubation increased fluorescence intensity of Rab32 into LDs and MT (Fig. 3E-L). FA incubation also up-regulated the protein expression of Rab32 in LDs and

MT (Fig. 3E-L). Rab32 was the only Rab GTPase associated with the MT, and also played the crucial role in controlling membrane trafficking. These result suggested that FA enhanced the localization of Rab32 in LDs and MT, which confirmed the close interaction between LDs and MT.

3.4. Creb-Pgc1α pathway regulated the FA-induced localization of Rab32 into LDs and MT, and mitochondrial biogenesis

To further determine the role of Creb, Pgc1α and Rab32 on FA-induced mitochondrial biogenesis, we used the specific inhibitors of Creb-Pgc1α pathway (666-15 for Creb and SR-18292 for Pgc1α, respectively). First, 666-15 and SR-18292 pre-treatment not only alleviated the FA-induced up-regulation of mRNA and protein expression of Creb and Pgc1α, but also significantly alleviated the FA-induced up-regulation of mRNA and protein expression of Rab32 (Supplementary Fig. 5 A-H). Furthermore, the FA-induced localization of Rab32 into LDs and MT were also significantly reduced by SR-18292 (Supplementary Fig. 5A-H), indicating the regulatory role of Creb and Pgc1α in FA-induced localization of Rab32 into LDs and MT. Moreover, the activator ZLN005 showed the opposite effect on FA-induced alteration of mitochondrial biogenesis. ZLN005 significantly increased the mitochondrial gene expression (Supplementary Fig. 6A). On the other hand, 666-15 suppressed Pgc1α protein expression, and SR-18292 did not inhibit Creb protein expression (Supplementary Fig. 5 A-H). ZLN005 up-regulated Pgc1α protein expression, but did not significantly influence Creb protein expression (Supplementary Fig. 6 B and C). Given that coactivator of Creb (TORC) was the most potent activator for Pgc1α [12], we speculated the essential regulatory role of Creb for Pgc1α expression.

Then, we further tested the role of the Creb-Pgc1α pathway on FA -induced alteration of mitochondrial biogenesis. As shown in Fig. 4A-C, both 666-15 and SR-18292 significantly attenuated the FA-induced increase of mRNA abundance of genes involved in mitochondrial biogenesis and also significantly down-regulated FA-induced mtDNA increase, indicating that the Creb-Pgc1α pathway was essential for FA-induced mitochondrial biogenesis. These results were further confirmed by the reduced fluorescence intensity of MT after 666-15 and SR-18292 treatments (Fig. 4D-E). Taken together, these data showed that the Creb-Pgc1α pathway regulated FA-induced localization of Rab32 into LDs and MT, and also regulated FA-induced mitochondrial biogenesis.

3.5. Creb-Pgc1α pathway controlled FA-induced enhancement of mitochondrial fusion & oxidation

After determining that the Creb-Pgc1α pathway regulated FA-induced enhancement of mitochondrial biogenesis, we tested the potential role of the Creb-Pgc1α pathway in regulating FA-mediated mitochondrial fusion and oxidation. We found that FA incubation increased MMP, ATP content and COX activity (Fig. 5A-D), suggesting that FA increased mitochondrial oxidation. Meanwhile, 48-h FA incubation up-regulated the protein levels of Cox-1 and Mnf1 (Fig. 5E-G). This result was further corroborated by the FA-induced up-regulation of mRNA abundances for genes involved in mitochondrial oxidation, including *cox-1*, *cox-2*, *cpt1*, *acox1* and *acadm* (Fig. 5H). FA incubation also up-regulated the mRNA abundance of genes involved in mitochondrial fusion, including *fis1*, *mfn1*, *mfn2*, *mid49* and *mid51* (Fig. 5I). These data indicated that FA incubation enhanced mitochondrial fusion and oxidation.

Next, we further investigated the role of the Creb-Pgc1α pathway on FA-induced enhancement of mitochondrial fusion and oxidation. SR-18292 pretreatment (specific inhibitor for Pgc1α) suppressed the FA-induced enhancement of mitochondrial fusion and oxidation, as shown in these changes of MMP, ATP content, COX activity, and mRNA abundance of genes involved in mitochondrial oxidation and fusion (Fig. 6A-E). Thus, the Creb-Pgc1α pathway controlled FA-induced enhancement of mitochondrial fusion and oxidation.

3.6. Creb-Pgc1α pathway was involved in Plin5-Atgl-mediated LDs lipolysis after FA incubation

We next explored the mechanism of the Creb-Pgc1α pathway influencing LDs lipolysis after FA incubation, and investigated the potential crosstalk between Creb-Pgc1α pathway-mediated mitochondrial biogenesis and Plin5-Atgl-mediated LDs lipolysis. First, we found the intracellular co-localization for Plin5 and Atgl (Fig. 7A), suggesting the potential Plin5-Atgl interaction. Furthermore, FA incubation increased the co-localization of Plin5 and Atgl, suggesting that FA intensified the Plin5-Atgl interaction. Moreover, FA incubation significantly increased Atgl protein level and decreased Plin5 protein level (Fig. 7 B & C). FA incubation significantly increased *atgl* mRNA level and decreased *plin5* mRNA level (Fig. 7D). Given that DAG and glycerine were key intermediates for LDs lipolysis, FA incubation increased the levels of TAG, DAG and glycerine, further indicating the FA-induced activation of LDs lipolysis (Fig. 7E). These data suggested that Plin5 and Atgl mediated FA-induced LDs lipolysis.

SR-18292 (specific inhibitor for Pgc1α) pretreatment attenuated the FA-induced

effects on expression of Atgl and Plin5 as well as on levels of TAG, DAG and glycerine, suggesting the direct involvement of the Creb-Pgc1α pathway in FA-induced LDs lipolysis (Fig. 8A-E). In contrast, both 666-15 and SR-18292 pretreatments exacerbated the FA-induced LDs accumulation (Fig. 8D-E), indicating that the inhibition of Creb-Pgc1α pathway aggravated FA-induced LDs accumulation. Given the close connection between LDs and MT and their crucial role in regulating lipid metabolism, we speculated that inhibition of the Creb-Pgc1α pathway prevented FA-induced mitochondrial biogenesis and activity, which in turn reduced FA-induced activation of LDs lipolysis.

3.7. The effect and mechanism of FA incubation influencing mitochondrial function and lipolytic metabolism in HepG2 cell line

To compare the similarity between mammals and yellow catfish, we further measured the FA-induced alteration of mitochondrial metabolism and lipolysis in HepG2 cell line (Supplementary Fig. 7). In agreement with the results in primary hepatocytes of *P. fulvidraco*, FA incubation increased the transcription of genes involved in mitochondrial metabolism, lipolysis and FA oxidation (Supplementary Fig. 7A), the protein expression levels of Creb and Pgc1α (Supplementary Fig. 7 B and C), and TAG, DAG and glycerine contents (Supplementary Fig. 7D). Furthermore, the FA-induced alterations were significantly suppressed by Pgc-1α inhibitor (Supplementary Fig. 7E and F). These results suggested the similarity between HepG2 cell line and primary hepatocytes of *P. fulvidraco*.

4. Discussion

Hepatic steatosis is the common chronic liver disease in vertebrate animals, and is characterized by excessive lipid accumulation in hepatocytes. In spite of the known role of LDs and mitochondria on hepatic lipid homeostasis, and the close interactions of these two components [4], the regulatory mechanism of LDs-MT interactions in lipid metabolism are unclear. Our present study reveals a novel mechanism underlying Creb-Pgc1α pathway mediating HFD- and FA-induced changes of LDs-MT interactions which in turns help LDs lipolysis.

The present study indicated that HFD and FA incubation markedly induced LDs accumulation, in agreement with other studies [28]. Thus, the biosynthesis and accumulation of triglyceride in livers and hepatocytes was still the main event triggered by high-fat diet feeding. Lipoprotein metabolism and VLDL-triglyceride secretion play an important role in HFD-induced hepatic steatosis. In this study, the mRNA abundances of LDL-R and VLDL-R were also increased by HFD, similar to other studies [45], indicating the potential role of VLDL in HFD-induced hepatic LDs accumulation. We further showed that HFD enhanced the LD proteins-mediated TAG deposition, similar to other reports [17]. Studies suggested that hepatocytes synthesized and stored TAG in the form of LDs [46]. Thus, stimulation of LD proteins-mediated TAG biosynthesis process was the prime driver of HFD-induced hepatic LDs accumulation. Interestingly, we also found that HFD stimulated LD proteins-mediated lipolysis and FA oxidation process. Given that lipolysis and subsequent FA oxidation were the key processes of hepatic lipid catabolism [47], we speculated that this process was an adaptive shift for hepatocytes in an attempt to alleviate HFD-induced LDs accumulation, in agreement with the report by Hodson et al [48]. Mitochondria was the main

site of fatty acid ß-oxidation and kept close interactions with LDs for hepatic lipid homeostasis [4]. We further explored the roles of mitochondria in FA-induced changes of LDs accumulation and lipid metabolism. Our study indicated that HFD and FA incubation stimulated mitochondrial biogenesis, and enhanced the fusion and oxidation of MT. Similarly, Ruggiero et al [49] suggested that HFD induced an adaptation of mitochondrial bioenergetics. Thus, our present study indicated that HFD and FA incubation induced hepatocellular LDs accumulation and mitochondrial biogenesis, and enhanced mitochondrial function.

To further elucidate the molecular mechanism of FA-induced stimulation of mitochondrial biogenesis and function, we explored the role of Creb and Pgc1α in these processes. Pgc-1α was a master regulator for mitochondrial biogenesis and function [9] and also controlled the expression of LD proteins in the liver [11]. Thus, Pgc1α was a potential link between LDs homeostasis and mitochondrial function. Our present study demonstrated that inhibition/activation of Pgc-1α blocked/activated the FA-induced mitochondrial biogenesis, showing that Pgc1α mediated the FA-induced mitochondrial biogenesis. Similarly, Aharoni-Simon et al [50] highlighted that PGC1α was associated with fatty liver-induced mitochondrial biogenesis in mice. Our study also showed that the inhibition of Creb was accompanied by the suppression of Pgc-1α; however, the inhibition of Pgc-1α had no effect on Creb expression. Furthermore, the activation of Pgc-1α had no positive effect on Creb expression. These observations indicated that Creb was the regulatory factor for Pgc-1α and mediated FA-induced mitochondrial biogenesis and function. Similarly, Chowanadisai et al [51] indicated the pyrroloquinoline quinone-induced stimulation of mitochondrial

510 biogenesis through CREB phosphorylation and increased PGC-1α expression. Other studies
511 indicated that TORC, a coactivator of Creb, was a strong inducer of *pgc-1α* gene
512 transcription [12]. Thus, our study indicated that Creb-Pgc1α pathway mediated FA-induced
513 mitochondrial biogenesis and function.

514 Having identified a close relationship between LD accumulation and mitochondrial
515 biogenesis after FA incubation, we further investigated the molecular mechanism of
516 FA-induced interaction of LDs and mitochondria. It has been reported that Rab proteins
517 enhanced the interactions between LDs and mitochondria [19, 52]. However, the role of
518 Rabs in the context of FA-induced interaction of LDs and mitochondria has not been
519 described before. The present study indicated that HFD up-regulated the expression of
520 several Rab proteins, suggesting a potential involvement of Rabs in HFD-induced
521 interactions between LDs and mitochondria. Bui et al [20] pointed out that Rab32 is the only
522 Rab GTPase associated with the mitochondria. Here, we found that HFD up-regulated the
523 mRNA and protein expression of Rab32 by more than two-fold and that FA incubation
524 resulted in the localization of Rab32 into LDs and mitochondria. Thus, these result indicated
525 an involvement of Rab32 in FA-induced interaction of LDs and mitochondria. Similarly,
526 Wang et al [46] found that multiple Rab proteins could regulate the dynamics of LDs. For
527 example, Rab32 affected lipid storage [53]. Alto et al [54] pointed out that Rab32 was
528 localized to MT and functioned as an A-kinase anchoring protein to regulate mitochondrial
529 dynamics. We also found that the localization of Rab32 into LDs and MT was blocked by
530 inhibition of the Creb-Pgc-1α pathway, indicating that Creb-Pgc-1α pathway was essential
531 for FA-induced localization of Rab32 into LDs and mitochondria.

Lipolysis and mitochondrial β-oxidation are critical metabolic pathways contributing to energy homeostasis through degradation of TAG stored in LDs [55]. Lipolysis involves protein trafficking and specific protein-protein interactions at the surface of LDs. Studies suggested that perilipin A (Plin), a lipid droplet scaffold protein, played a central role in orchestrating interactions among lipolytic effector proteins [56]. Plin5 negatively regulates lipolysis and FA oxidation, contributing to TAG accumulation [27]. Atgl is the rate-limiting enzyme in TAG hydrolysis in most organs and cells [57]. The present study indicated that HFD activated the LDs proteins-mediated lipolysis process, up-regulated the mRNA and protein expression of Atgl, but down-regulated the transcript and protein expression of Plin5. Moreover, we found that FA incubation significantly enhanced the intracellular co-localization of Plin5 and Atgl, suggesting a direct Plin5-Atgl interactions under FA incubation. Similarly, Granneman et al [58] pointed out that Plin controlled lipolysis by its interaction with Atgl. Moreover, Granneman et al [59] suggested that Plin5 acted in coordinating Atgl activity. Thus, FA/HFD-activated LDs lipolysis occurred via the interaction between Plin5 and Atgl.

Creb was the upstream regulator of lipid metabolism [13] and mediated mitochondrial gene expression [14]. Therefore, we next investigated the role of the Creb-Pgc-1α pathway in Plin5-Atgl-mediated lipolysis of LDs. We found that the inhibition/stimulation of the Creb-Pgc1α pathway blocked/activated the FA-induced alteration of Plin5 and Atgl, indicating that the Creb-Pgc1α pathway was responsible for these changes. The inhibition/stimulation of the Creb-Pgc1α pathway also prevented/ aggravated the FA-induced TAG hydrolysis as evidenced by the increasing DAG and glycerine levels. DAG and

554 glycerine were two main intermediate products of LDs lipolysis [60]. From these data, we
555 thought that the Creb-Pgc1α pathway was required for Plin5-Atgl-mediated LDs lipolysis
556 during FA incubation. Thus, under HFD and FA incubation, Creb-Pgc1α pathway activated
557 mitochondrial biogenesis, fusion and oxidation, increased the interaction between LDs and
558 mitochondria, and finally enhanced Plin5-Atgl-mediated LDs lipolysis. The up-regulation of
559 LDs lipolysis was regarded as an adaptive shift for hepatocytes in an attempt to alleviate
560 FA-induced LDs accumulation. Similarly, other studies indicated the close crosstalk among
561 FA trafficking, LDs lipolysis and mitochondrial function [61], and the crucial role of Pgc1α,
562 Plin5 and Atgl in linking LDs lipolysis and mitochondrial function [62, 63]. Moreover, our
563 study also indicated the similarity in FA-induced changes of mitochondrial metabolism,
564 lipolysis and FA oxidation between mammals and yellow catfish, including that our results
565 in yellow catfish can be potentially extrapolated to mammals.

566 In conclusion, in this work, HFD and FA activated Creb-Pgc1α-mediated
567 mitochondrial biogenesis, fusion and oxidation, increased interactions of LDs-MT, which in
568 turn activated Atgl-Plin5-mediated LDs lipolysis in hepatocytes and accordingly alleviated
569 HFD- and FA-induced lipid accumulation. The present study underlied HFD-induced
570 LDs-MT interaction and their role in hepatic lipid homeostasis, which provided potential
571 targets for intervention and prevention of hepatic steatosis.

572 **Conflict of Interest**

573 The authors declared that they had no conflicts of interest with the contents of this
574 article.

Authors' contributions

Song Y.F. and Luo Z. designed the experiment. Song Y.F. conducted the experiment and data analysis with the help of Ling S.C. and Chen G.H. Hogstrand C. and Luo Z. provided some critical suggestions for data analysis. Song Y.F. drafted the manuscript. Hogstrand C. and Luo Z. revised the manuscript. All the authors reviewed and approved the manuscript.

Acknowledgments

This work was supported by the National Key R&D Program of China (grant no.: 2018YFD0900400), National Natural Science Foundation of China (grant no. 31902380), the Fundamental Research Funds for the Central Universities, China (grant no. 2662018PY089) and China Postdoctoral Science Foundation (grant no. 2016M602326).

References

[1] Carr RM, Ahima RS. Pathophysiology of lipid droplet proteins in liver diseases. Exp Cell Res. 2016;340:187-192. DOI: org/10.1016/j.yexcr.2015.10.021.

[2] Fabbrini E, Magkos F. Hepatic steatosis as a marker of metabolic dysfunction. Nutrients. 2015;7: 4995-5019. DOI: org/10.3390/nu7064995.

[3] Gluchowski NL, Becuwe M, Walther TC, Farese Jr RV. Lipid droplets and liver disease: from basic biology to clinical implications. Nat Rev Gastroenterol Hepatol. 2017;14:343. DOI: 10.1038/nrgastro.2017.32.

596 [4] Barbosa AD, Savage DB, Siniossoglou S. Lipid droplet–organelle interactions: emerging
597 roles in lipid metabolism. Curr Opin Cell Biol. 2015;35:91-97. DOI:
598 10.1016/j.ceb.2015.04.017.
599 [5] Mashek DG, Khan SAA, Sathyanarayan J, Ploeger M, Franklin MP. Hepatic lipid droplet
600 biology: getting to the root of fatty liver. Hepatology. 2015;62:964-967. DOI:
601 10.1002/hep.27839.
602 [6] Sunny NE, Bril F, Cusi K. Mitochondrial adaptation in nonalcoholic fatty liver disease:
603 novel mechanisms and treatment strategies. Trends Endocrinol Metab. 2017;28: 250-260.
604 DOI: 10.1016/j.tem.2016.11.006.
605 [7] Barbosa AD, Siniossoglou S. Function of lipid droplet-organelle interactions in lipid
606 homeostasis. Biochim Biophys Acta Mol Cell Res. 2017;1864:1459-1468. DOI:
607 10.1016/j.bbamcr.2017.04.001.
608 [8] Couvillion MT, Soto IC, Shipkovenska G, Churchman LS. Synchronized mitochondrial
609 and cytosolic translation programs. Nature. 2016;533:499-503. DOI:
610 10.1038/nature18015.
611 [9] Lagouge M, Argmann C, Gerhart-Hines Z, Meziane H, Lerin C, Daussin F. Resveratrol
612 improves mitochondrial function and protects against metabolic disease by activating
613 SIRT1 and PGC-1α. Cell. 2006;127:1109-1122. DOI: 10.1016/j.cell.2006.11.013
614 [10] Li X, Monks B, Ge Q, Birnbaum MJ. Akt/PKB regulates hepatic metabolism by
615 directly inhibiting PGC-1α transcription coactivator. Nature. 2007;447:1012. DOI:
616 10.1038/nature05861.
617 [11] Hallberg M, Morganstein DL, Kiskinis E, Shah K, Kralli A, Dilworth SM. A functional

618 interaction between RIP140 and PGC-1α regulates the expression of the lipid droplet
619 protein CIDEA. Mol Cell Biol. 2008;28:6785-6795. DOI: 10.1128/MCB.00504-08.
620 [12] Wu Z, Huang X, Huang Y, Feng C, Handschin Y, Feng P, Gullicksen S, Stevenson SC.
621 Transducer of regulated CREB-binding proteins (TORCs) induce PGC-1α transcription
622 and mitochondrial biogenesis in muscle cells. Proc Natl Acad Sci.
623 2006;103:14379-14384. DOI: 10.1073/pnas.0606714103.
624 [13] Han J, Li E, Chen L, Zhang Y, Wei F, Liu J, Wang Y. The CREB coactivator CRTC2
625 controls hepatic lipid metabolism by regulating SREBP1. Nature. 2015;524:243-246.
626 DOI: 10.1038/nature14557.
627 [14] Shanmughapriya S, Rajan S, Hoffman NE, Zhang X, Guo S, Kolesar JE, Baba Y. Ca^{2+}
628 signals regulate mitochondrial metabolism by stimulating CREB-mediated expression of
629 the mitochondrial Ca^{2+} uniporter gene MCU. Sci Signal. 2015;8:ra23-ra23. DOI:
630 10.1126/scisignal.2005673.
631 [15] Nguyen MK, Kim CY, Kim JM, Park BO, Lee S, Park H, Do Heo W. Optogenetic
632 oligomerization of Rab GTPases regulates intracellular membrane trafficking. Nat Chem
633 Biol. 2016;12: 431-436. DOI: 10.1038/nchembio.2064.
634 [16] Kiss RS, Nilsson T. Rab proteins implicated in lipid storage and mobilization. J Biomed
635 Res. 2014;28:169-177. DOI: 10.7555/JBR.28.20140029.
636 [17] Liu M, Ge R, Liu W, Liu Q, Xia X, Lai M. Differential proteomics profiling identifies
637 LDPs and biological functions in high-fat diet-induced fatty livers. J Lipid Res.
638 2017;58:681-694. DOI: 10.1194/jlr.M071407.
639 [18] Zehmer JK, Huang Y, Peng G, Pu J, Anderson RG, Liu P. A role for lipid droplets in

640 inter-membrane lipid traffic. Proteomics. 2009;9:14-921. DOI:
641 10.1002/pmic.200800584.
642 [19] Pu J, Ha CW, Zhang S, Jung JP, Huh WK, Liu P. Interactomic study on interaction
643 between lipid droplets and mitochondria. Protein Cell. 2011;2:487-496. DOI:
644 10.1007/s13238-011-1061-y.
645 [20] Bui M, Gilady SY, Fitzsimmons RE, Benson MD, Lynes EM, Gesson K. Rab32
646 modulates apoptosis onset and mitochondria-associated membrane (MAM) properties. J
647 Biol Chem. 2010;285:31590-31602. DOI: 10.1074/jbc.M110.101584.
648 [21] Meyer A, Van de Peer Y. From 2R to 3R: evidence for a fish-specific genome
649 duplication (FSGD). Bioessays 2015;27:937-945. DOI: 10.1002/bies.20293.
650 [22] Gong G, Dan C, Xiao S, Guo W, Huang P, Xiong Y. Chromosomal-level assembly of
651 yellow catfish genome using third-generation DNA sequencing and Hi-C analysis.
652 GigaScience. 2018;7: DOI: 10.1093/gigascience/giy120.
653 [23] Wei CC, Wu K, Gao Y, Zhang LH, Li DD, Luo Z. Magnesium reduces hepatic lipid
654 accumulation in yellow catfish (*Pelteobagrus fulvidraco*) and modulates lipogenesis and
655 lipolysis via PPARA, JAK-STAT, and AMPK pathways in hepatocytes. J Nutr.
656 2017;147:1070-1078. DOI: 10.3945/jn.116.245852.
657 [24] Song YF, Hogstrand C, Wei CC, Wu K, Pan YX, Luo Z. Endoplasmic reticulum (ER)
658 stress and cAMP/PKA pathway mediated Zn-induced hepatic lipolysis. Environ Pollut.
659 2017;228:256-264. DOI: 10.1016/j.envpol.2017.05.046.
660 [25] Song YF, Luo, Z, Zhang LH, Hogstrand C, Pan YX. Endoplasmic reticulum stress and
661 disturbed calcium homeostasis are involved in copper-induced alteration in hepatic lipid

662 metabolism in yellow catfish *Pelteobagrus fulvidraco*. Chemosphere. 2016;144:
663 2443-2453. DOI: 10.1016/j.chemosphere.2015.11.031.
664 [26] Goo YH, Son SH, Paul A. Lipid droplet-associated hydrolase promotes lipid droplet
665 fusion and enhances ATGL degradation and triglyceride accumulation. Sci Rep. 2017;7:
666 2743. DOI: 10.1038/s41598-017-02963-y.
667 [27] Wang C, Zhao Y, Gao X, Li L, Yuan Y, Liu F. Perilipin 5 improves hepatic lipotoxicity
668 by inhibiting lipolysis. Hepatology. 2015;61:870-882. DOI: 10.1002/hep.27409.
669 [28] Ling SC, Wu K, Zhang DG, Luo Z. Endoplasmic reticulum stress–mediated autophagy
670 and apoptosis alleviate dietary fat–induced triglyceride accumulation in the Intestine and
671 in isolated intestinal epithelial cells of yellow catfish. J Nutr. 2019;DOI:
672 doi.org/10.1093/jn/nxz135.
673 [29] Sharabi K, Lin H, Tavares CDJ, Dominy JE, Camporez JP, Perry RJ, et al. Selective
674 chemical inhibition of pgc-1α gluconeogenic activity ameliorates type 2 diabetes. Cell
675 2017;169:148-160.e15.
676 [30] Song YF, Xu YH, Zhuo MQ, Wu K, Luo Z. CREB element is essential for unfolded
677 protein response (UPR) mediating the Cu-induced changes of hepatic lipogenic
678 metabolism in Chinese yellow catfish (*Pelteobagrus fulvidraco*). Aquat. Toxicol.
679 2018:203:69-79.
680 [31] Xu Y, Kabba JA, Ruan W, Wang Y, Zhao S, Song X, Pang T. The PGC-1α activator
681 ZLN005 ameliorates ischemia-induced neuronal injury *in vitro* and *in vivo*. Cell. Mol.
682 Neurobiol. 2018:38:929-939.
683 [32] Ricchi M, Odoardi MR, Carulli L, Anzivino C, Ballestri S, Pinetti A, Fantoni LI, Marra

684 F, Bertolotti M, Banni S. Differential effect of oleic and palmitic acid on lipid
685 accumulation and apoptosis in cultured hepatocytes. J. Gastroenterol. Hepatol.
686 2009;24:830-840.
687 [33] Song YF, Gao Y, Hogstrand C, Li DD, Pan YX, Luo Z. Upstream regulators of
688 apoptosis mediates methionine-induced changes of lipid metabolism. Cell Signalling
689 2018;51:176-190. DOI: 10.1016/j.cellsig.2018.08.005.
690 [34] Shevchenko A, Tomas H, Havli J, Olsen JV, Mann M. In-gel digestion for mass
691 spectrometric characterization of proteins and proteomes. Nat Protoc. 2006;1: 2856-2860.
692 DOI: 10.1038/nprot.2006.468.
693 [35] Michalski A, Damoc E, Hauschild JP, Lange O, Wieghaus A, Makarov A. Mass
694 spectrometry-based proteomics using Q Exactive, a high-performance benchtop
695 quadrupole Orbitrap mass spectrometer. Mol Cell Proteomics. 2011;10:M111-011015.
696 DOI: 10.1074/mcp.M111.011015.
697 [36] Marchese A. Monitoring Chemokine Receptor Trafficking by Confocal
698 Immunofluorescence Microscopy. Methods Enzymol. 2016;570:281-292.
699 [37] Schutte B, Nuydens R, Geerts H, Ramaekers F. Annexin V binding assay as a tool to
700 measure apoptosis in differentiated neuronal cells. J Neurosci Methods. 1998;86: 63-69.
701 DOI: 10.1016/s0165-0270(98)00147-2.
702 [38] Pan YX, Luo Z, Zhuo MQ, Wei CC, Chen GH. Oxidative stress and mitochondrial
703 dysfunction mediated Cd-induced hepatic lipid accumulation in zebrafish *Danio rerio*.
704 Aquat Toxicol. 2018;199:12-20. DOI: 10.1016/j.aquatox.2018.03.017.
705 [39] Tan XY, Luo Z, Xie P, Li XD, Liu XJ, Xi WQ. Effect of dietary conjugated linoleic

706 acid (CLA) on growth performance, body composition and hepatic intermediary
707 metabolism in juvenile yellow catfish *Pelteobagrus fulvidraco*. Aquaculture.
708 2010;310:186-191. DOI: 10.1016/j.aquaculture.2010.10.011.
709 [40] Xin G, Wei Z, Ji C, Zheng H, Gu J, Ma L. Xanthohumol isolated from *Humulus lupulus*
710 prevents thrombosis without increased bleeding risk by inhibiting platelet activation and
711 mtDNA release. Free Radic Biol Med. 2017;108:247-257. DOI:
712 10.1016/j.freeradbiomed.2017.02.018.
713 [41] West AP, Khoury-Hanold W, Staron M, Tal MC, Pineda CM, Lang SM. Mitochondrial
714 DNA stress primes the antiviral innate immune response. Nature. 2015;520:553-557.
715 DOI: 10.1038/nature14156.
716 [42] Nakahira K, Kyung SY, Rogers AJ, Gazourian L, Youn S, Massaro AF. Circulating
717 mitochondrial DNA in patients in the ICU as a marker of mortality: derivation and
718 validation. PLoS Med. 2013;10:e1001577. DOI: 10.1371/journal.pmed.1001577.
719 [43] Vandesompele J, De Preter K, Pattyn F, Poppe B, Van Roy N, De Paepe A. Accurate
720 normalization of real-time quantitative RT-PCR data by geometric averaging of multiple
721 internal control genes. Genome Biol. 2002;3: research0034-1. DOI:
722 10.1186/gb-2002-3-7-research0034.
723 [44] Stenmark H. Rab GTPases as coordinators of vesicle traffic. Nat Rev Mol Cell Biol.
724 2009;10:513-525. DOI: 10.1038/nrm2728.
725 [45] Jordal AEO, Hordvik I, Pelsers M, Bernlohr DA, Torstensen BE. FABP3 and FABP10
726 in Atlantic salmon (*Salmo salar* L.)-General effects of dietary fatty acid composition and
727 life cycle variations. Comp. Biochem. Physiol. 2006;145:147-158.

728 [46] Wilfling F, Wang H, Haas JT, Krahmer N, Gould TJ, Uchida A. Triacylglycerol
729 synthesis enzymes mediate lipid droplet growth by relocalizing from the ER to lipid
730 droplets. Dev Cell. 2013;24:384-399. DOI: 10.1016/j.devcel.2013.01.013.
731 [47] Lass A, Zimmermann, R, Oberer, M, Zechner R. Lipolysis–a highly regulated
732 multi-enzyme complex mediates the catabolism of cellular fat stores. Prog Lipid Res.
733 2011;50:14-27. DOI: 10.1016/j.plipres.2010.10.004.
734 [48] Hodson L, McQuaid SE, Humphreys SM, Milne R, Fielding BA, Frayn KN. Greater
735 dietary fat oxidation in obese compared with lean men: an adaptive mechanism to
736 prevent liver fat accumulation?. Am J Physiol Endocrinol Metab. 2010;299:584-592.
737 DOI: 10.1152/ajpendo.00272.2010.
738 [49] Ruggiero C, Ehrenshaft M, Cleland E, Stadler K. High-fat diet induces an initial
739 adaptation of mitochondrial bioenergetics in the kidney despite evident oxidative stress
740 and mitochondrial ROS production. Am J Physiol Endocrinol Metab.
741 2011;300:1047-1058. DOI: 10.1152/ajpendo.00666.2010.
742 [50] Aharoni-Simon M, Hann-Obercyger M, Pen S, Madar Z, Tirosh O. Fatty liver is
743 associated with impaired activity of PPARγ-coactivator 1α (PGC1α) and mitochondrial
744 biogenesis in mice. Lab Invest. 2011;91:1018-1028. DOI: 10.1038/labinvest.2011.55.
745 [51] Chowanadisai W, Bauerly KA, Tchaparian E, Wong A, Cortopassi GA, Rucker RB.
746 Pyrroloquinoline quinone stimulates mitochondrial biogenesis through cAMP response
747 element-binding protein phosphorylation and increased PGC-1α expression. J Biol Chem.
748 2010;285:142-152. DOI: 10.1074/jbc.M109.030130.
749 [52] Gao Q, Goodman JM. The lipid droplet—a well-connected organelle. Front Cell Dev

Biol. 2015;3:49. DOI: 10.3389/fcell.2015.00049.

[53] Wang C, Liu Z, Huang X. Rab32 is important for autophagy and lipid storage in Drosophila. PLoS One 2012;7:e32086. DOI: 10.1371/journal.pone.0032086.

[54] Alto NM, Soderling J, and Scott, J. D. Rab32 is an A-kinase anchoring protein and participates in mitochondrial dynamics. J Cell Biol. 2002;158:659-668. DOI: 10.1083/jcb.200204081.

[55] Saponaro C, Gaggini M, Carli F, Gastaldelli A. The subtle balance between lipolysis and lipogenesis: a critical point in metabolic homeostasis. Nutrients. 2015;7:9453-9474. DOI: 10.3390/nu7115475.

[56] Brasaemle DL. Thematic review series: adipocyte biology. The perilipin family of structural lipid droplet proteins: stabilization of lipid droplets and control of lipolysis. J Lipid Res. 2007;48:2547-2559. DOI: 10.1194/jlr.R700014-JLR200.

[57] Eichmann TO, Kumari M, Haas JT, Farese RV, Zimmermann R, Lass A. Studies on the substrate and stereo/regioselectivity of adipose triglyceride lipase, hormone-sensitive lipase, and diacylglycerol-O-acyltransferases. J Biol Chem. 2012;287:41446-41457. DOI: 10.1074/jbc.M112.400416.

[58] Granneman JG, Moore HPH, Krishnamoorthy R, Rathod MX, Krishnamoorthy R, Rathod M. Perilipin controls lipolysis by regulating the interactions of AB-hydrolase containing 5 (Abhd5) and adipose triglyceride lipase (Atgl). J Biol Chem. 2011;284:34538-34544. DOI: 10.1074/jbc.M109.068478.

[59] Granneman JG, Moore HPH, Mottillo EP, Zhu Z, Zhou L. Interactions of perilipin-5 (Plin5) with adipose triglyceride lipase. J Biol Chem. 2011;286: 5126-5135. DOI:

10.1074/jbc.M110.180711.

[60] Serup AK, Alsted TJ, Jordy AB, Schjerling P, Holm C, Kiens B. Partial disruption of lipolysis increases postexercise insulin sensitivity in skeletal muscle despite accumulation of dag. Diabetes. 2016;65:2932-2942. DOI: 10.2337/db16-0655.

[61] Rambold AS, Cohen S, Lippincott-Schwartz J. Fatty acid trafficking in starved cells: regulation by lipid droplet lipolysis, autophagy, and mitochondrial fusion dynamics. Dev Cell. 2015;32:678-692. DOI: 10.1016/j.devcel.2015.01.029.

[62] Haemmerle G, Moustafa T, Woelkart G, Büttner S, Schmidt A, Van De Weijer T, Schreiber R. ATGL-mediated fat catabolism regulates cardiac mitochondrial function via PPAR-α and PGC-1. Nat Med. 2011;17:1076-1085. DOI: 10.1038/nm.2439.

[63] Kimmel AR, Sztalryd C. Perilipin 5, a lipid droplet protein adapted to mitochondrial energy utilization. Curr Opin Lipidol. 2014;25:110-117. DOI: 10.1097/MOL.0000000000000057.

Figure Legends:

Fig. 1. Differentially expressed LDs proteins in the livers of *P. fulvidraco* fed the control and HFD. A: Western blotting analysis to verify the representative LD proteins identified by hepatocellular LD sub-proteome. B: Quantitative analysis for relative gray value of western blotting using ImageJ software. C: Q-PCR to verify the representative genes coding LD proteins. Values are mean ± SEM (n= 3 replicate tanks). Asterisks indicated significant differences between the control and HFD group ($P< 0.05$).

Fig. 2. FA-induced hepatocellular LDs accumulation coincided with increasing mitochondrial biogenesis in hepatocytes of *P. fulvidraco*. A: Representative confocal microscopic image of hepatocellular LD (green) and mitochondria (red) (bars = 25 μm). B: percentage of cells with large LDs; C: LD volume; D: relative red intensity of fluorescence with different LD diameters; E: quantitative analysis for relative fluorescent intensity; F: size distribution. G: Representative EM image of hepatocellular LD and mitochondria (bars = 1μm), M, mitochondria; LD, lipid droplet. H & I: Quantitative analysis for the numbers of mitochondria per cell (H) and relative area of mitochondria/cytoplasm (I). J: Schematic representation of the colocalization between MTs and LDs; K: The transcription of genes involved in Creb-Pgc1α pathway and mitochondrial biogenesis. n indicated the number of cells used for counting. Different letters indicated significant differences among groups ($P< 0.05$).

Fig. 3. FA enhanced the expression levels of CREB and PGC1α, and the localization of Rab32 into LDs and MT in hepatocytes of *P. fulvidraco*. A, B & C: Western blotting analyzed the protein expression levels of Creb and Pgc1α, and quantitative analysis for relative gray value of western blotting using ImageJ software. D: The levels of cAMP. E: Co-localization analysis of Rab32 (red) and LD (green) (bars = 5 μm). F: Co-localization analysis of Rab32 (green) and mitochondria (red) (bars = 5 μm). G: Western blotting analyzed the protein expression of Rab32 in LDs. H: Western blotting analyzed the protein expression of Rab32 in mitochondria. I: Quantitative analysis for relative red intensity of fluorescence in E. J & K: Quantitative analysis for relative gray value of western blotting in G & H using ImageJ software. L: Quantitative analysis for relative green intensity of fluorescence in F. Values are mean ± SEM (n = 4 independent biological experiments).

Asterisks indicated significant differences between 0 h and 48 h group; different letters indicated significant differences among groups (P< 0.05).

Fig. 4. CREB-PGC1α pathway regulated FA-induced mitochondrial biogenesis in hepatocytes of *P. fulvidraco*. A: The levels of cAMP. B: The levels of mtDNA. C: The transcription of genes involved in Creb-Pgc1α pathway and mitochondrial biogenesis. D: Representative confocal microscopic image of hepatocellular mitochondria (red) (bars = 15 μm). E: Quantitative analysis for relative red intensity of fluorescence in L. Values are mean ± SEM (n = 4 independent biological experiments). Asterisks indicate significant differences between FA and FA + inhibitors group (P< 0.05).

Fig. 5. Creb-Pgc1α pathway controlled the FA-induced mitochondrial fusion in hepatocytes of *P. fulvidraco*. A: Images of hepatocytes stained by JC-1 output by fluorescence scanning confocal microscopy (bars = 25 μm) and flow cytometry analysis under FA and Pgc-1α inhibitor (SR-18292) incubation. B: Quantitative analysis for relative ratio of red/green fluorescence intensity. C: The ATP content; D: COX activity. E and F: The protein expression levels of Cox-1 (E) and Mnf1 (F). G: Quantitative analysis for relative gray value of western blotting in E and F using ImageJ software. H and I: The transcription of genes involved in mitochondrial oxidation (H) and fusion (I). Values are mean ± SEM (n = 4 independent biological experiments). Asterisks indicated significant differences between FA and FA + SR-18292 group; different letters indicated significant differences among groups (*P*< 0.05).

Fig. 6. Creb-Pgc1α pathway controlled the FA-induced mitochondrial oxidation in hepatocytes of *P. fulvidraco*. A: Quantitative analysis for relative ratio of red/green fluorescence intensity in Figure 5A. B & C: The ATP content (B) and COX activity (C). D & E: The transcription of genes involved in mitochondrial oxidation (D) and fusion (E). Values are mean ± SEM (n = 4 independent biological experiments). Asterisks indicated significant differences between FA and FA + SR-18292 group (P< 0.05).

Fig. 7. Plin5-Atgl-mediated LDs lipolysis in hepatocytes of *P. fulvidraco* after FA incubation. A: Co-localization analysis of Plin5 (red) and Atgl (green). B: The protein expression of Plin5 and Atgl in hepatocellular. C: Quantitative analysis for relative gray value of western blotting in B using ImageJ software. D: The transcription of *plin5* and *atgl*. E: The contents of TAG, DAG and glycerine (GI). Different letters indicated significant

differences among groups ($P< 0.05$).

Fig. 8. Involvement of Creb-Pgc1α pathway in Plin5-Atgl-mediated LDs lipolysis in hepatocytes of *P. fulvidraco* after FA incubation. A & B: The protein expression levels of Plin5 and Atgl in hepatocellular LD extraction (A), and quantitative analysis for relative gray value of western blotting using ImageJ software (B). C: The transcription of *plin5* and *atgl* in hepatocytes. D: Representative confocal microscopic image of hepatocellular LDs (green) (bar = 25 μm). E: The contents of TAG, DAG and glycerine (GI). Values are mean ± SEM (n = 4 independent biological experiments). Asterisks indicate significant differences between FA and FA + SR-18292 group ($P< 0.05$).

Figure 1.

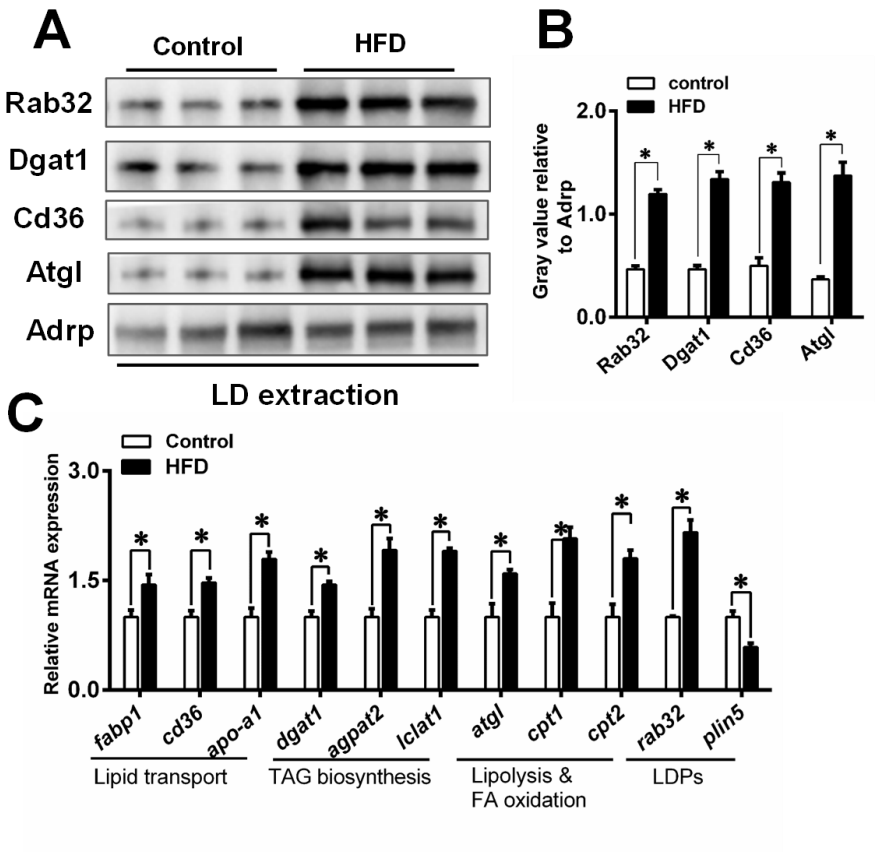
A
Control
HFD
Rab32
Dgat1
Cd36
Atgl
Adrp
LD extraction
B
control
HFD
Gray value relative to Adrp
2.0
1.0
0.0
Rab32
Dgat1
Cd36
Atgl
C
Control
HFD
Relative mRNA expression
3.0
1.5
0.0
fabp1
cd36
apo-a1
dgat1
agpat2
lclat1
atgl
cpt1
cpt2
rab32
plin5
Lipid transport
TAG biosynthesis
Lipolysis & FA oxidation
LDPs

Fig. 2.

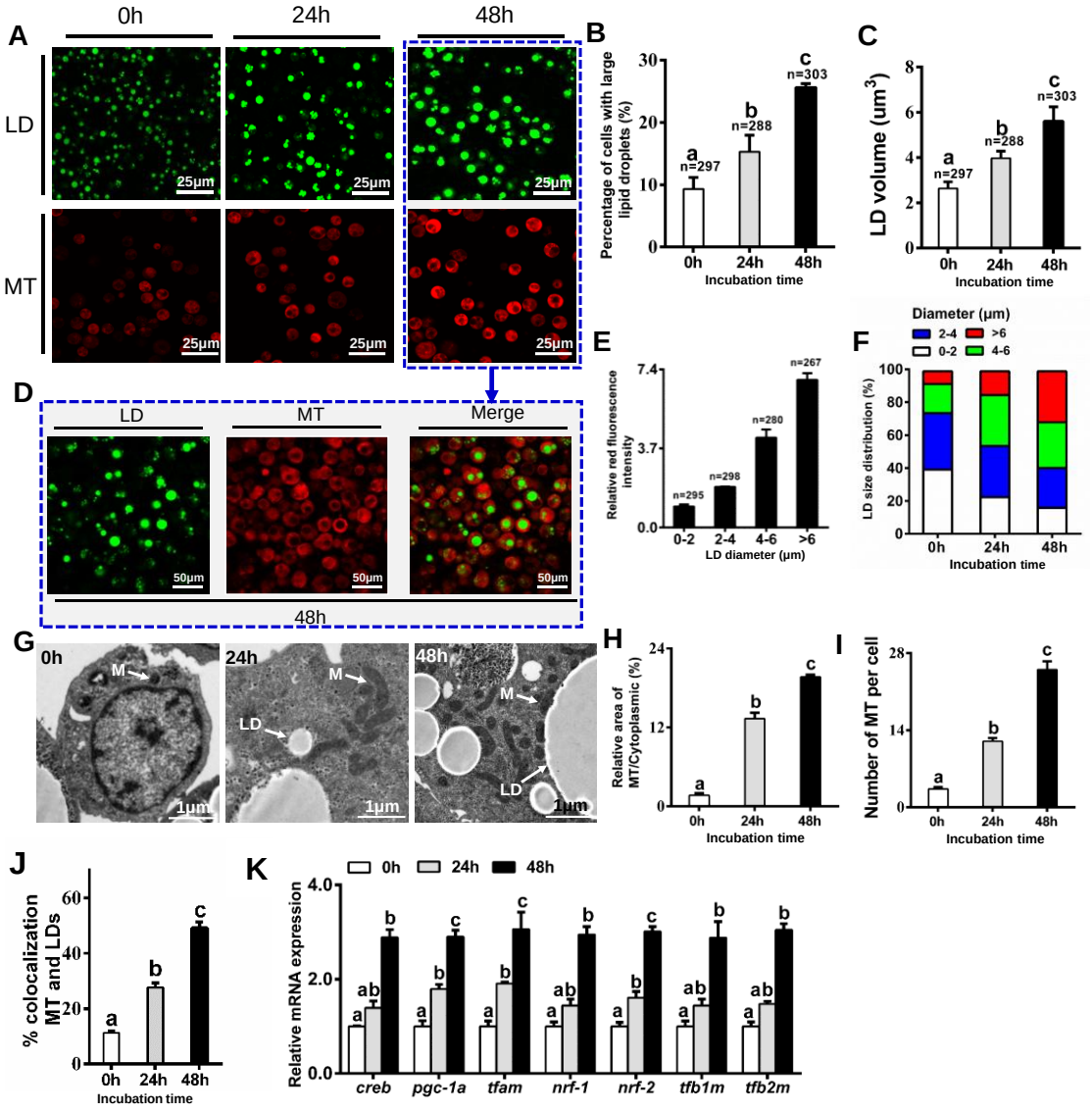
A
0h
24h
48h
LD
MT
25μm
B
Percentage of cells with large lipid droplets (%)
Incubation time
C
LD volume (um3)
D
LD
MT
Merge
50μm
48h
E
Relative red fluorescence intensity
LD diameter (μm)
F
Diameter (μm)
2-4
>6
0-2
4-6
LD size distribution (%)
G
M
LD
1μm
H
Relative area of MT/Cytoplasmic (%)
I
Number of MT per cell
J
% colocalization MT and LDs
K
Relative mRNA expression
creb
pgc-1a
tfam
nrf-1
nrf-2
tfb1m
tfb2m

Fig. 3.

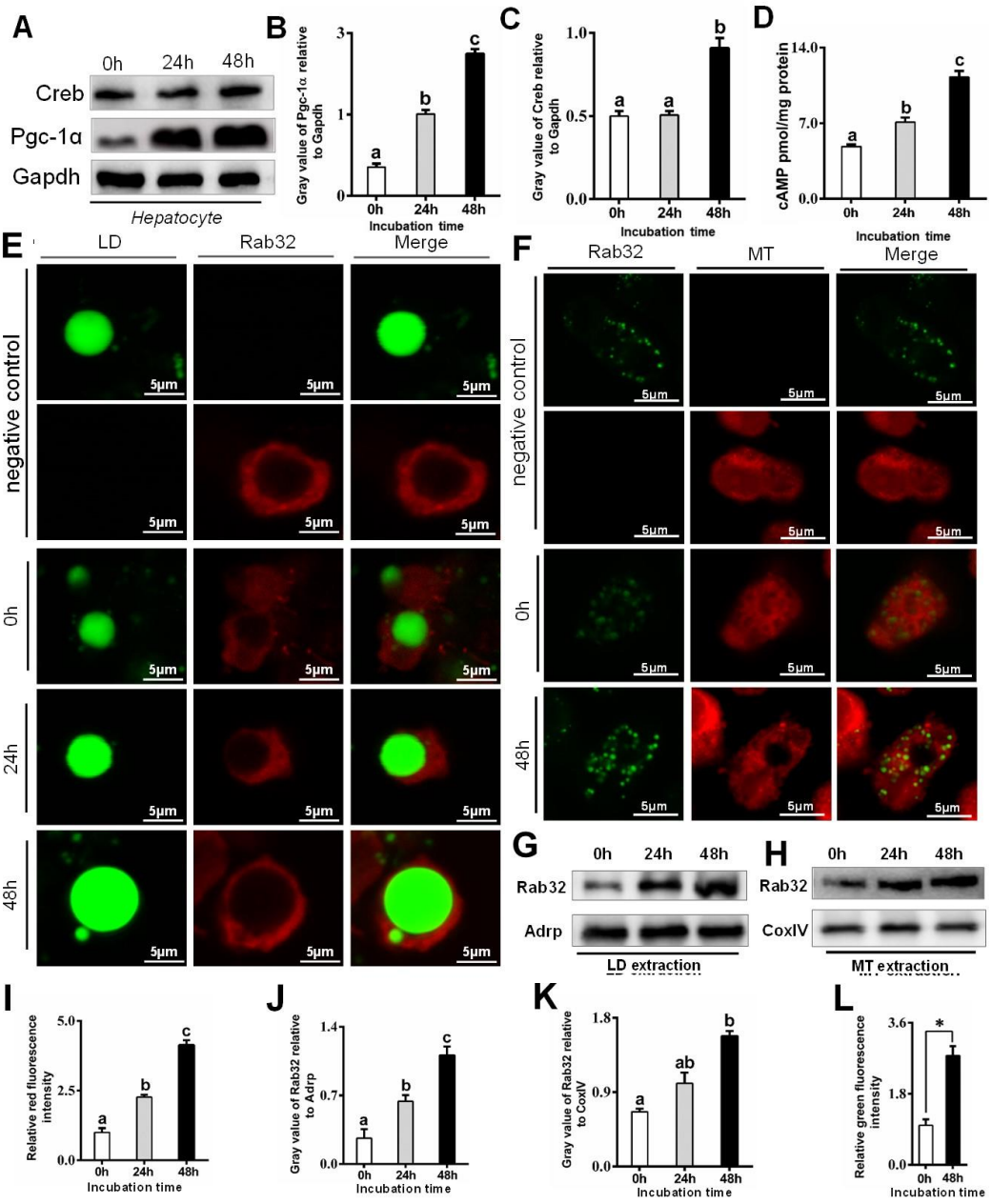
A
0h
24h
48h
Creb
Pgc-1α
Gapdh
Hepatocyte
B
Gray value of Pgc-1α relative to Gapdh
Incubation time
C
Gray value of Creb relative to Gapdh
Incubation time
D
cAMP pmol/mg protein
Incubation time
E
LD
Rab32
Merge
negative control
0h
24h
48h
5μm
F
Rab32
MT
Merge
G
Rab32
Adrp
LD extraction
H
Rab32
CoxIV
MT extraction
I
Relative red fluorescence intensity
Incubation time
J
Gray value of Rab32 relative to Adrp
Incubation time
K
Gray value of Rab32 relative to CoxIV
Incubation time
L
Relative green fluorescence intensity
Incubation time

Fig. 4.

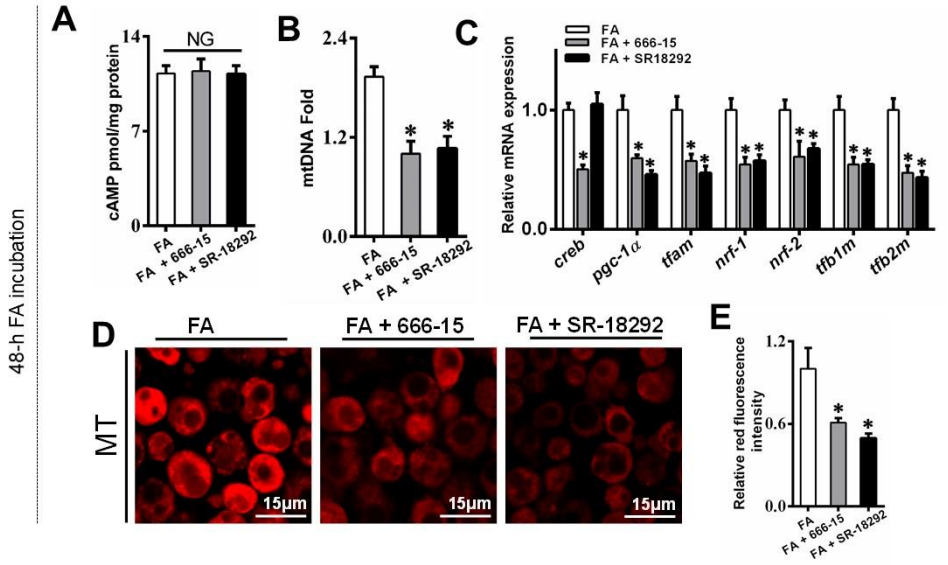
48-h FA incubation
A
NG
cAMP pmol/mg protein
14
7
0
FA
FA + 666-15
FA + SR-18292
B
mtDNA Fold
2.4
1.2
0.0
C
FA
FA + 666-15
FA + SR18292
Relative mRNA expression
1.0
0.0
creb
pgc-1α
tfam
nrf-1
nrf-2
tfb1m
tfb2m
D
FA
FA + 666-15
FA + SR-18292
MT
15μm
E
Relative red fluorescence intensity
1.2
0.6
0.0

966

967 **Fig. 5.**

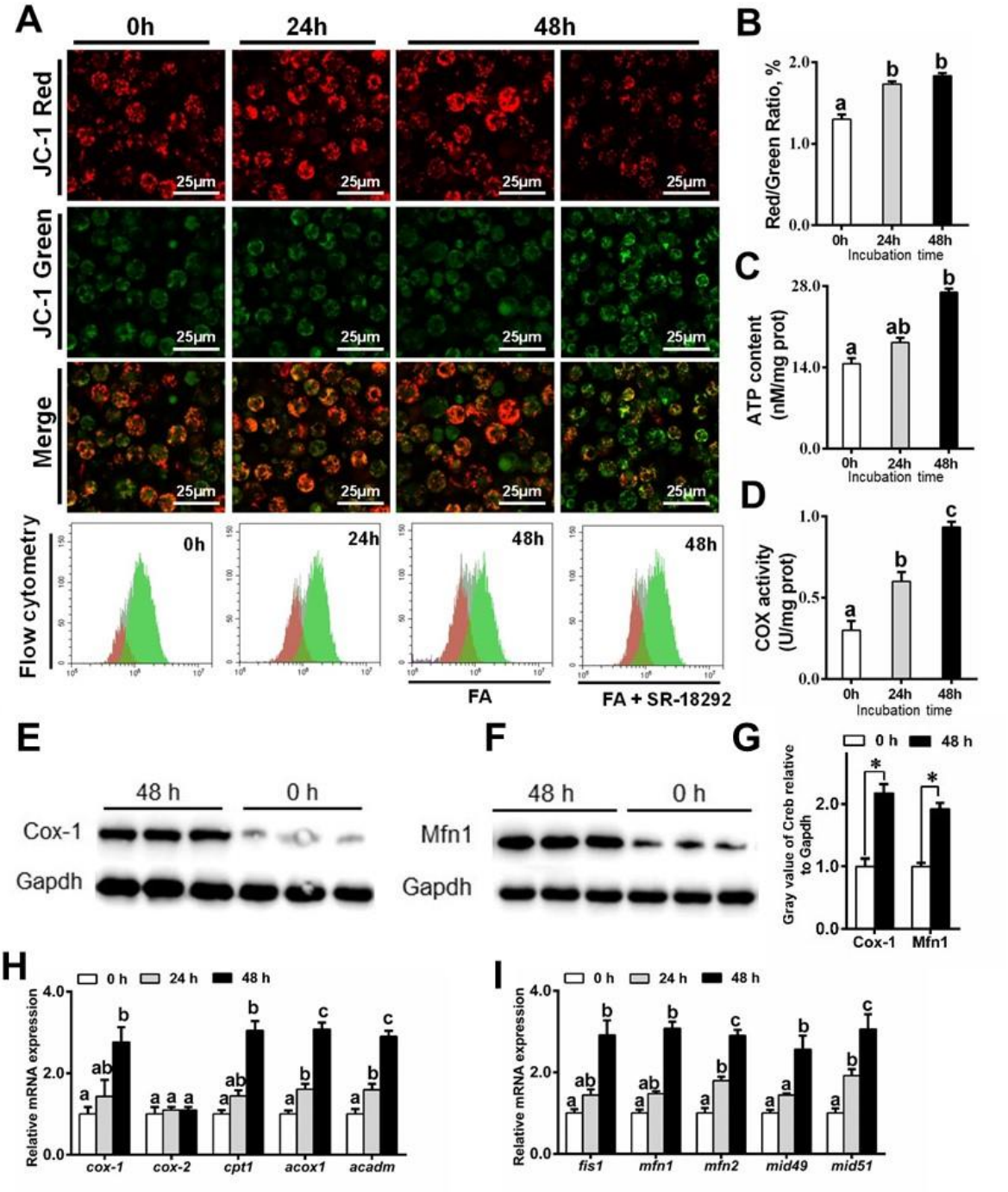

968

969

970

Fig. 6.

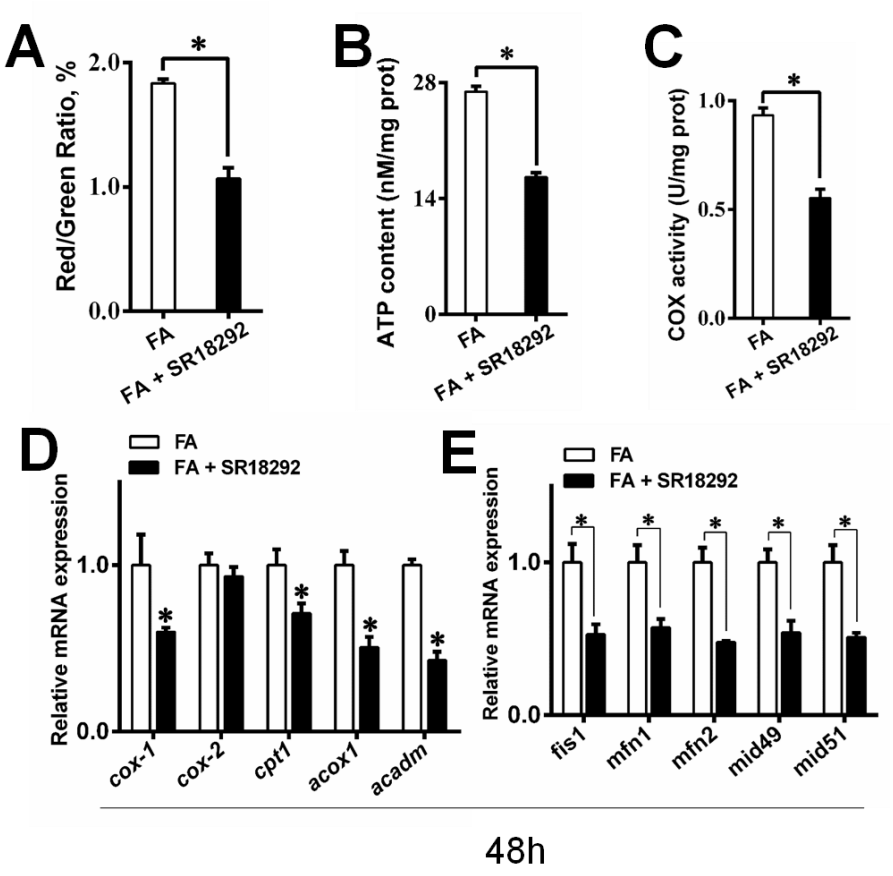
A
Red/Green Ratio, %
2.0
1.0
0.0
FA
FA + SR18292
B
ATP content (nM/mg prot)
28
14
0
FA
FA + SR18292
C
COX activity (U/mg prot)
1.0
0.5
0.0
FA
FA + SR18292
D
FA
FA + SR18292
Relative mRNA expression
1.0
0.0
cox-1
cox-2
cpt1
acox1
acadm
E
FA
FA + SR18292
Relative mRNA expression
1.0
0.0
fis1
mfn1
mfn2
mid49
mid51
48h

Fig. 7.

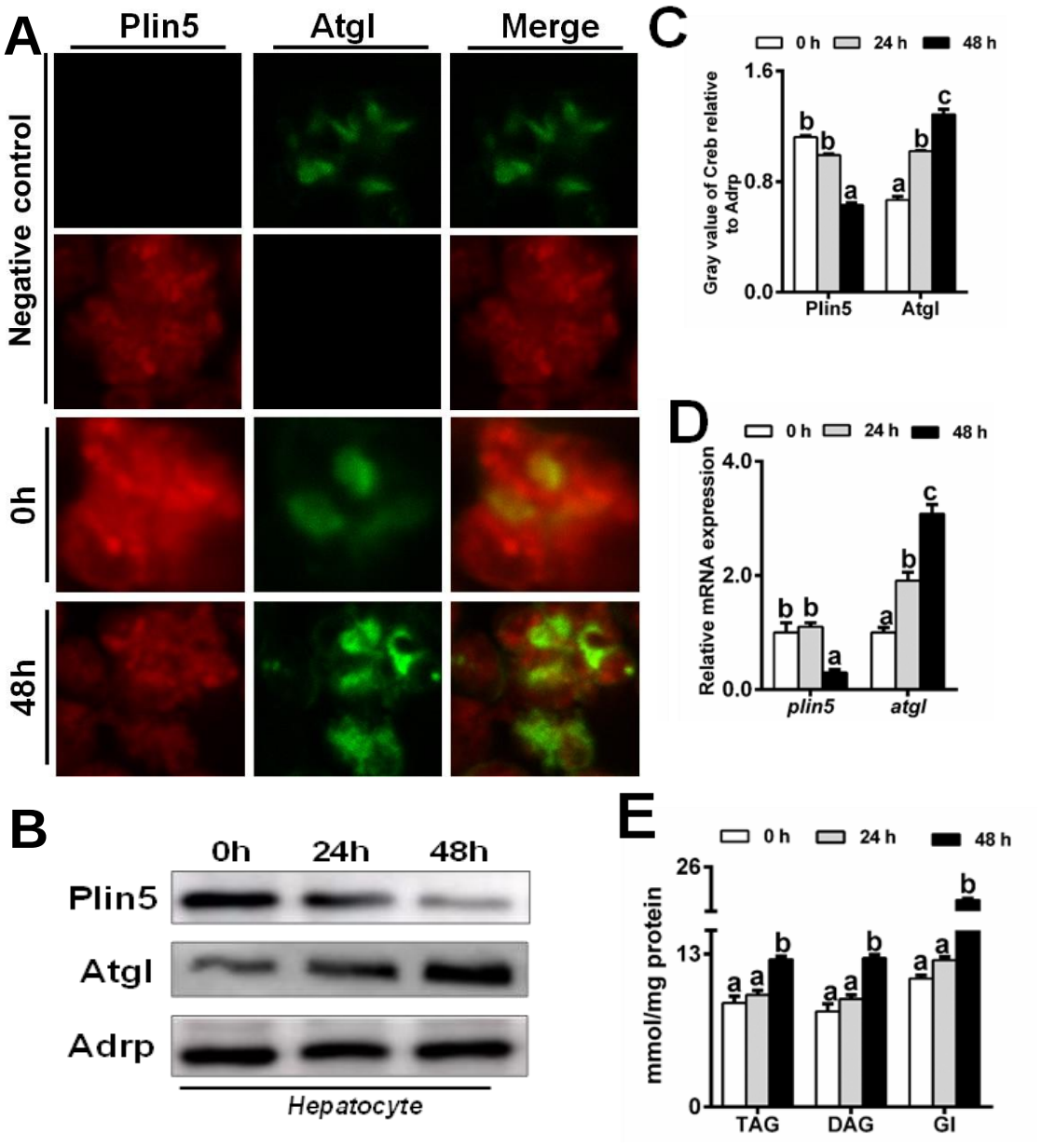
A
Plin5
Atgl
Merge
Negative control
0h
48h
B
0h
24h
48h
Plin5
Atgl
Adrp
Hepatocyte
C
0 h
24 h
48 h
Gray value of Creb relative to Adrp
1.6
0.8
0.0
Plin5
Atgl
D
Relative mRNA expression
4.0
2.0
0.0
plin5
atgl
E
mmol/mg protein
26
13
0
TAG
DAG
GI

Fig. 8.

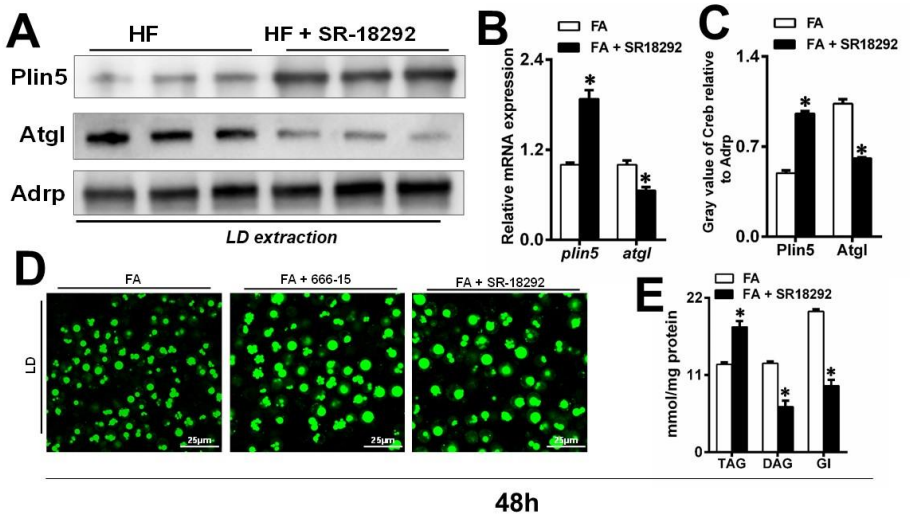
A
HF
HF + SR-18292
Plin5
Atgl
Adrp
LD extraction
B
FA
FA + SR18292
Relative mRNA expression
2.4
1.2
0.0
plin5
atgl
C
FA
FA + SR18292
Gray value of Creb relative to Adrp
1.4
0.7
0.0
Plin5
Atgl
D
FA
FA + 666-15
FA + SR-18292
LD
25μm
E
FA
FA + SR18292
mmol/mg protein
22
11
0
TAG
DAG
GI
48h